A Novel Plasmonic Sensor Based on Dual-Channel D-Shaped Photonic Crystal Fiber for Enhanced Sensitivity in Simultaneous Detection of Different Analytes

J. Divya, S. Selvendran, A. Sivanantha Raja, and Vamsi Borra

***Abstract*— A dual-channel D-shaped photonic crystal fiber (PCF) based plasmonic sensor is proposed in this paper for the simultaneous detection of two different analytes using the surface plasmon resonance (SPR) technique. The sensor employs a 50 nm-thick layer of chemically stable gold on both cleaved surfaces of the PCF to induce the SPR effect. This configuration offers superior sensitivity and rapid response, making it highly effective for sensing applications. Numerical investigations are conducted using the finite element method (FEM). After optimizing the structural parameters, the sensor exhibits a maximum wavelength sensitivity of 10000 nm/RIU and an amplitude sensitivity of −216 RIU^{-1} between the two channels. Additionally, each channel of the sensor exhibits its unique maximal wavelength and amplitude sensitivities for different refractive index (RI) ranges. Both channels demonstrate a maximal wavelength sensitivity of 6000 nm/RIU. In the RI range of 1.31-1.41, Channel 1 (Ch1) and Channel 2 (Ch2) achieved their maximum amplitude sensitivities of $-85.39RIU^{-1}$ and -304.52 RIU^{-1}, respectively, with a resolution of 5×10^{-5}. This sensor structure is noteworthy for its ability to measure both amplitude and wavelength sensitivity, providing enhanced performance characteristics suitable for various sensing purposes in chemical, biomedical, and industrial fields.**

***Index Terms*— Photonic crystal fiber, surface plasmon resonance, sensor, gold, wavelength sensitivity, amplitude sensitivity.**

I. Introduction

THE SPR technique is a method that progressively measures molecular interactions in real-time that occur in close proximity to a metal surface [1]. Due to its broad sensing range, simple light feeding, and control over propagation, the SPR-based sensing technique is more feasible than other sensing techniques [2]. Kretschmann et al. first proposed a prism-based SPR technique to measure variations in the RI of surrounding medium(analyte). This method utilizes thin metal layers placed between a glass prism and the analyte to induce the plasmon effect. The commonly used plasmonic metals in this technique are gold and silver [3]. Complete reflection happens when plane-polarized light hits a glass prism beyond a critical angle. At a specific angle and wavelength, an evanescent field is generated between the glass and metal layer, which is known as the resonance condition. At resonance condition, the incident light penetrates the metal surface, generating an evanescent field. The incident light excites free electrons in the metal-dielectric interface, leading to the formation of surface plasmons. As a result, the reflected light intensity decays exponentially, which is known as the SPR effect [4].

The propagation characteristics of surface plasmons are extremely sensitive to the RI of the analyte near the metal surface [5]. If any minute RI changes in the analyte cause deviations in the phase or amplitude of the reflected light. Hence RI variation of the analyte near the metal surface, can be easily detected by using this SPR method. SPR sensors have diverse uses in sensing, such as chemical sensing [6], biosensing [7], environmental monitoring [8], and biochemical application [9]. The main drawback of this method is it is not portable because of its bulky size, so it cannot be used in remote sensing applications, and the cost of this sensor is also high [10].

In order to address these problems, SPR sensors for remote sensing applications use optical fibers instead of prisms due to their compact size, exceptional sensitivity, and superior accuracy [11]. The downside of this sensor is the metallization of the fiber structure. In order to accomplish the metallization, the cladding portion of conventional fibers should be polished almost to the core. It degrades the structure's integrity and results in mechanical breakdowns. It also increases the cost of fabrication. Hassani et al. proposed an initial SPR sensor using PCF as a remedy for these concerns, as metals are coated or filled in a specific air hole in PCF structures [12]. PCFs have gained significant attention in the past few decades due to their unique optical properties, including high birefringence,

Manuscript received 19 March 2023; revised 11 May 2023 and 10 June 2023; accepted 23 June 2023. Date of publication 11 July 2023; date of current version 3 January 2024. This work was supported in part by the Vellore Institute of Technology (VIT) through the "VIT RGEMS SEED GRANT" and in part by the Leadership and Management of Vellore Institute of Technology Chennai under its Research Promotion Scheme. *(Corresponding author: S. Selvendran.)*

J. Divya and S. Selvendran are with the School of Electronics Engineering (SENSE), Vellore Institute of Technology, Chennai, Tamil Nadu 600127, India (e-mail: selvendran.s@vit.ac.in).

A. Sivanantha Raja is with the Department of Electronics and Communication Engineering (ECE), Alagappa Chettiar Government College of Engineering and Technology, Karaikudi, Tamil Nadu 630003, India.

Vamsi Borra is with the Department of Electrical and Computer Engineering, Rayen School of Engineering-College of STEM, Youngstown State University, Youngstown, OH 44555 USA.

Digital Object Identifier 10.1109/TNB.2023.3294330

low transmission loss, strong non-linearity, endless single mode, and the ability to control light propagation [13]. These properties make PCFs ideal for various sensing applications, including chemical sensing [14], gas sensing [15], temperature sensing [16], and biosensing [17]. In recent years, there has been a significant research focus on utilizing the SPR technique in combination with PCF for sensor applications due to its unique advantages.

The core mode and plasmon mode coupling at the metal-dielectric interface is the underlying principle of a SPR-based PCF sensor [18]. This coupling creates leaky modes in the guided core mode, happening at a certain wavelength when the effective indices(n_{eff}) of both modes are almost the same, causing the plasmon mode to receive the majority of energy from the core mode, leading to the phase matching condition that generates the resonance wavelength [19]. The RI of the analyte varies near the metal layer causing the resonant wavelength shift. This wavelength shift scheme provides higher sensitivity and accuracy. Depending on where the analyte is positioned within the sensor structure, sensing techniques are categorized as either internal sensing [20] or external sensing [21]. Yang et al. created a PCF sensor utilizing SPR method with a gold-graphene configuration, where gold acted as the plasmonic substance and graphene was incorporated to enhance sensor efficiency. By situating the analyte exterior to the fiber structure, the sensor obtained a wavelength sensitivity of 4200 nm/RIU and an amplitude sensitivity of 450 RIU^{-1}, within a detection range of 1.32-1.41 [22]. Rahaman et al. designed a SPR sensor utilizing a PCF to estimate the glucose level in urine samples. A thin layer of gold was coated in the cladding region of the fiber to generate SPR effect, and the sensor was plunged in the sample for measurements. The SPR sensor's maximal achieved amplitude, and wavelength sensitivity were 152 RIU^{-1} and 2500 nm/RIU, respectively [23].

All of these sensors were developed to analyze one analyte at a time, which requires more time and resources. The multi-channel/multi-analyte sensing approach has the advantage of simultaneously detecting multiple analytes in a same sensor structure, which minimizes the need for analyte filling, emptying, and cleaning stages and thus reduces time and cost. Zhang et al. developed the first-ever multi-channel micro structured fiber-based SPR sensor, which can simultaneously detect multiple analytes, thereby resolving the limitation of single-channel sensors. The sensor exhibited outstanding wavelength sensitivity of 1535 nm/RIU at a detection range of 1.33-1.36 [24]. PCF-based multi-channel SPR sensors have gained popularity among researchers for multi-analyte sensing applications in recent times. In 2015, Otupiri et al. introduced a multi-channel PCF sensor utilizing SPR method that combined circular and elliptical air holes in the cladding region of the PCF to attain great birefringence. The sensor demonstrated high wavelength sensitivity of 4600 nm/RIU for Ch1, and 2300 nm/RIU for Ch2 through the dual coating of gold and Ta_2TO_5 on the inner wall of the cladding region [5]. It will be challenging to fabricate both circular and elliptical air holes together. In 2019, Kaur et al. presented a dual-channel PCF-based SPR sensor that demonstrated exceptional wavelength sensitivity. Ch1 and Ch 2 displayed optimal wavelength sensitivity of 1000 nm/RIU and 3750 nm/RIU, respectively, between the RI values of 1.30-1.40.The sensor consisted of an analyte channel made up of two concentric rings coated with gold on the outside to create a plasmonic layer [25]. Yasli et al. suggested a multi-channel SPR sensor in 2020, which obtained an optimal wavelength sensitivity of 2500 nm/RIU for Ch1 and 3083 nm/RIU for Ch2. The flat surface of the analyte channel was covered with a plasmonic coating made of gold and silver. Graphene was layered on top of the silver in order to safeguard it from oxidation and enhance sensitivity [26]. In that year, Yasli et al. offered an PCF-based another multi channel SPR sensor with enhanced sensitivity of 4250 nm/RIU for Ch1 and 4200 nm/RIU for Ch2.The inner walls of Ch1, and Ch2 were coated with gold and silver, respectively, to act as plasmonic layers and generate plasmonic effects [27]. Recently, Kamrunnahar et al. proposed a PCF based dual channel SPR sensor in 2022, where gold was coated as a plasmonic layer to induce SPR. The obtained highest sensitivity of Ch1 was 25000 nm/RIU and 3000 nm/RIU for Ch2 [28].

Moreover, in certain aforementioned studies, filling or coating metals in the inner wall of cladding is challenging, and it is observed that few channels performed unevenly with lower sensitivity. Therefore, further research is required to develop a multi-channel sensor with high sensitivity, quality factor and consistent performance across all channels. Thus, the proposed work presents a dual channel D-shape PCF sensor, utilizing the SPR technique for simultaneous detection of two different substances. The sensor structure involves removal of top and bottom circular parts of the fiber, forming a dual D-shape structure, and coating the cleaved surfaces with a slender layer of gold. FEM is utilized for fine-tuning the sensor structure for maximum sensitivity. The optimized sensor has a wavelength sensitivity of 10000 nm/RIU and an amplitude sensitivity of -216 RIU^{-1} between its two channels, Ch1 and Ch2. Both channels exhibit a peak wavelength sensitivity of 6000 nm/RIU, with a resolution of 5×10^{-5}, across the detection range of 1.31 to 1.41.

II. Proposed SPR Sensor Structure and Theory

Fig.1(a) shows a visual depiction of a proposed SPR based dual channel D-shaped PCF sensor. The cladding section of the sensor has a hexagonal shape, and includes air holes arranged in a triangular pattern with a diameter (d) of 0.5 μm. The pitch or lattice constant (Λ) between these holes is 0.8 μm. Dual core is used in this structure to analyze two different analytes at the same time and the core region is formed by removing two airhole rings in the top and one air hole ring in the bottom side. Birefringence induced by varying core size through reducing second ring of air holes by half of the initial size. This reduces the core size, as a large core permits multi-mode operation [29]. A dual D-shape is formed by slicing off the top and bottom circular portions of the PCF, and thin plasmonic layer of gold (t_{Au}) with a thickness of 0.05 μm is layered on the cleaved section of the PCF to induce the SPR

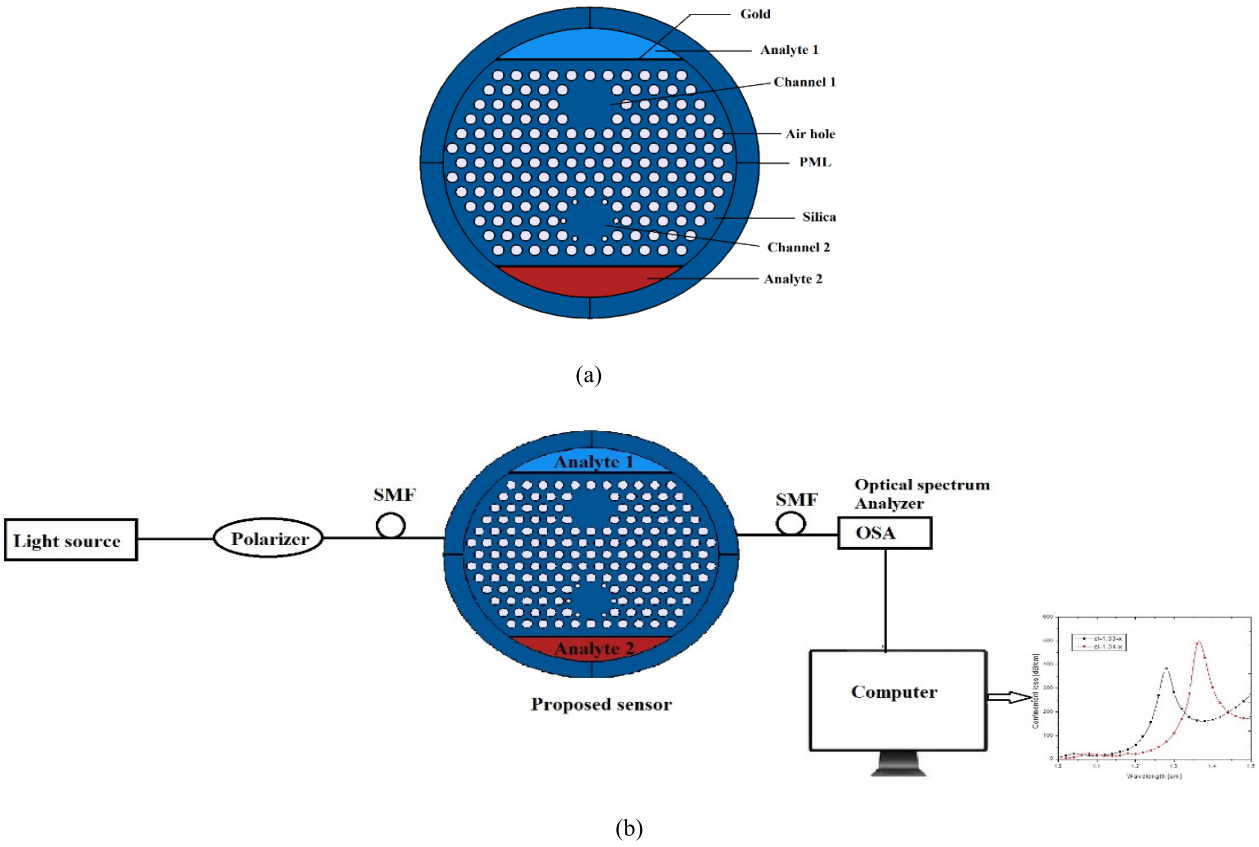

Fig. 1. (a) Graphical representation of the proposed dual channel D-shaped PCF sensor using SPR; (b) Experimental arrangement of the proposed sensor.

effect. In the outer region, 1μm thick perfectly matched layer (t_{PML}) is used and that is ~10% of the total diameter of this sensor i.e., 7.4μm. The analyte is placed between the gold layer and the PML, two sensing channels- Ch1 at the top and Ch2 at the bottom are used to detect two different analytes. Applying a scattering boundary condition on the exterior of the structure leads to a further reduction in the amount of reflected energy.

The proposed sensor uses silica as its core material and its RI of silica is determined by Sellmeier equation [20].

$$n\left(\lambda\right)^2 = 1 + \frac{A_1\lambda^2}{\lambda^2 - \lambda_1^2} + \frac{A_2\lambda^2}{\lambda^2 - \lambda_2^2} + \frac{A_3\lambda^2}{\lambda^2 - \lambda_3^2}$$

The Sellmeier constants for the proposed sensor are A1 = 0.696 1663, A2 = 0.407 9426, A3 = 0.897 479, $\lambda 1$ = 0.068 404, $\lambda 2$ = 0.116 2414, $\lambda 3$ = 9.896 161 where λ represents the operating wavelength in μm.

Gold is chosen as the plasmonic material due to its excellent optical characteristics, stability, and biocompatibility. The Drude model is commonly employed to predict the dispersion behavior of gold at different wavelengths. Mathematically, it can be represented as follows [19],

$$\varepsilon = 1 - \frac{\omega_P^2}{\omega^2 + i\omega\Gamma_P}$$

where plasma frequency ω_P = 9.06eV and damping rate Γ_P = 0.07eV.

Fig. 1(b) illustrates the experimental arrangement of the dual channel D-shaped sensor proposed. In order to enhance coupling efficiency, a light source with a broad spectrum is introduced into the sensor through single mode fiber (SMF). The inclusion of a polarizer helps to enhance the visibility of confinement loss for a particular polarization. By manipulating the RI of the analyte that is added to the sensor, there will be changes in the intensity or the wavelength of the confinement loss spectrum. These changes can be detected by connecting an optical spectrum analyzer (OSA) to a computer. The RI of the unknown analyte can be determined by analyzing the data received from the computer.

Numerical analyze are carried out using FEM method. For obtain precise results, a physics-controlled mesh model has been utilized to mesh the sensor's structure with extremely fine element sizes. The mesh consists of elements with a maximum element size of 0.52640 μm and a minimum element size of 0.00111 μm. The maximum element growth rate is set to 1.25, while the vertex elements have a size of 692. Ch1 is composed of 72009 total elements, including 5567 boundary elements, and has a minimum element quality of 0.4612. Ch2 comprises 84522 total elements, with 5602 boundary elements and a minimum element quality of 0.5385. The defective modes of the PCF are responsible for its convergence error, which are affected by perturbations with compact support [30]. However, the convergence error can be significantly reduced by using the proposed SPR based dual channel D-shaped PCF structure. The error has been measured to be 1.5×10^{-5} at 1.36 μm and

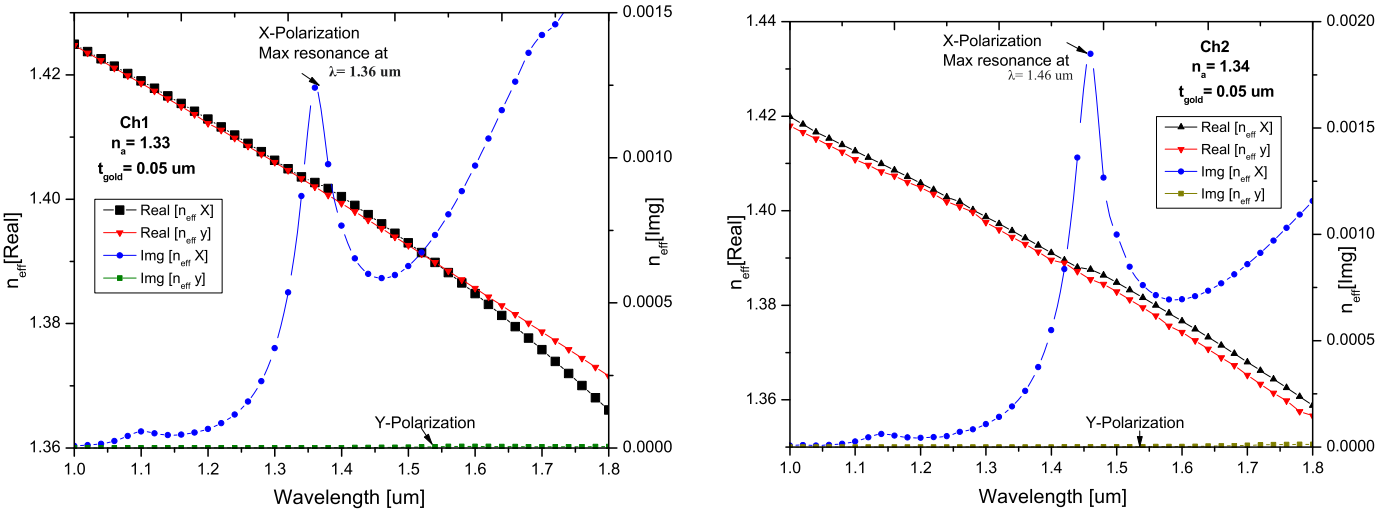

(a) (b)

Fig. 2. Dispersion relation between the real and the imaginary parts of n_{eff} as a function of wavelength: (a) Ch1; (b) Ch2.

9.7×10^{-4} at 1.46 μm, and it decreases with higher iteration numbers.

The proposed dual side polished D-shaped PCF based SPR sensor is fabricated using stack and draw method [31], the D-shape is obtained by using side polishing method [32], and the polished region is coated with a thin layer of gold using the chemical vapor deposition (CVD) method [33]. Finally, an infiltration method is utilized to inject the analyte into the sensing channels [34].

III. Results and Discussion

The effectiveness of the dual-channel D-shaped SPR sensor proposed in this study is closely tied to its geometric parameters, such as the diameter of the air holes, pitch size, and thickness of the gold layer. Through careful optimization of these parameters, the sensor's performance can be significantly enhanced. To evaluate the influence of each parameter, they are individually varied while maintaining the other structural parameters constant. Confinement loss is a crucial parameter because it can significantly impact the sensitivity and accuracy of the optical sensors. It measures the extent of light that is attenuated when it is propagate within the core region of the PCF [35]. The confinement loss equation can be expressed as follows [19]:

$$\text{Confinement loss} = 8.686\text{x}\frac{2\Pi}{\lambda}\text{x Im}(n_{eff})\text{x}10^4(\text{dB/cm}).$$

where Im (n_{eff}) - imaginary part of the effective mode index, λ- operating wavelength in μm.

A. Transmission Characteristics and Dispersion Relation of the Proposed Sensor

Transmission characteristics of the proposed SPR based D-shaped dual channel PCF sensor are investigated for the wavelength range of 1.0μm $-$1.8μm Figs. 2 (a, b) illustrates the relationship between the dispersion characteristics of the effective refractive index (n_{eff}) for Ch1 and Ch2, with respect to their real and imaginary components.

With increasing wavelength, the real part of the n_{eff} for the core-guided mode decreases in both Ch1 and Ch2. At a specific wavelength of 1.36μm, energy is transferred to the plasmon mode from the core guided mode, leading to a slight decrease in real part of the Ch1. This suggests the initiation of the resonance condition, where the imaginary component of the n_{eff} achieves its optimal value. Similarly, the resonance wavelength of Ch2 is at 1.46μm, where it reaches its maximum value. Ch1 allows the multi-mode propagation because of its core size is greater than Ch2's core size; as a result, Ch1's signal strength is lesser than Ch2's. As is evident from Fig. 2(a, b) the coupling efficiency of the Y-polarized modes is significantly lower than that of the X-polarized modes in both Ch1 and Ch2. As a result, for further analysis of both channels, the X-polarized mode has chosen over the Y-polarized mode.

Figs. 3(a, b) display the electric field distribution of the proposed sensor for Ch1 and Ch2, respectively. Fig.3.a, b (i, ii) illustrates the X and Y-polarization, respectively, when the incident light is guided through the core. The coupling mode and plasmon mode are depicted in Fig. 3.a, b (iii, iv). The couple mode refers to the condition where the phase-matching criterion is fulfilled, resulting in the maximum transfer of energy from the core mode to the plasmon mode [36].

B. Optimization of Plasmonic Materials

Incorporating plasmonic materials, such as gold [23], silver [37], copper [38], aluminium [39], and titanium [40] with a PCF structure can alter the properties of the guided modes of the fiber through their interaction. This interaction can lead to an improvement in light confinement, a reduction in losses, and an enhancement of nonlinear effects, making it a promising technique for various applications. Among these materials, silver and gold exhibit favorable optical properties, low material losses, and high resonance peaks. However, gold

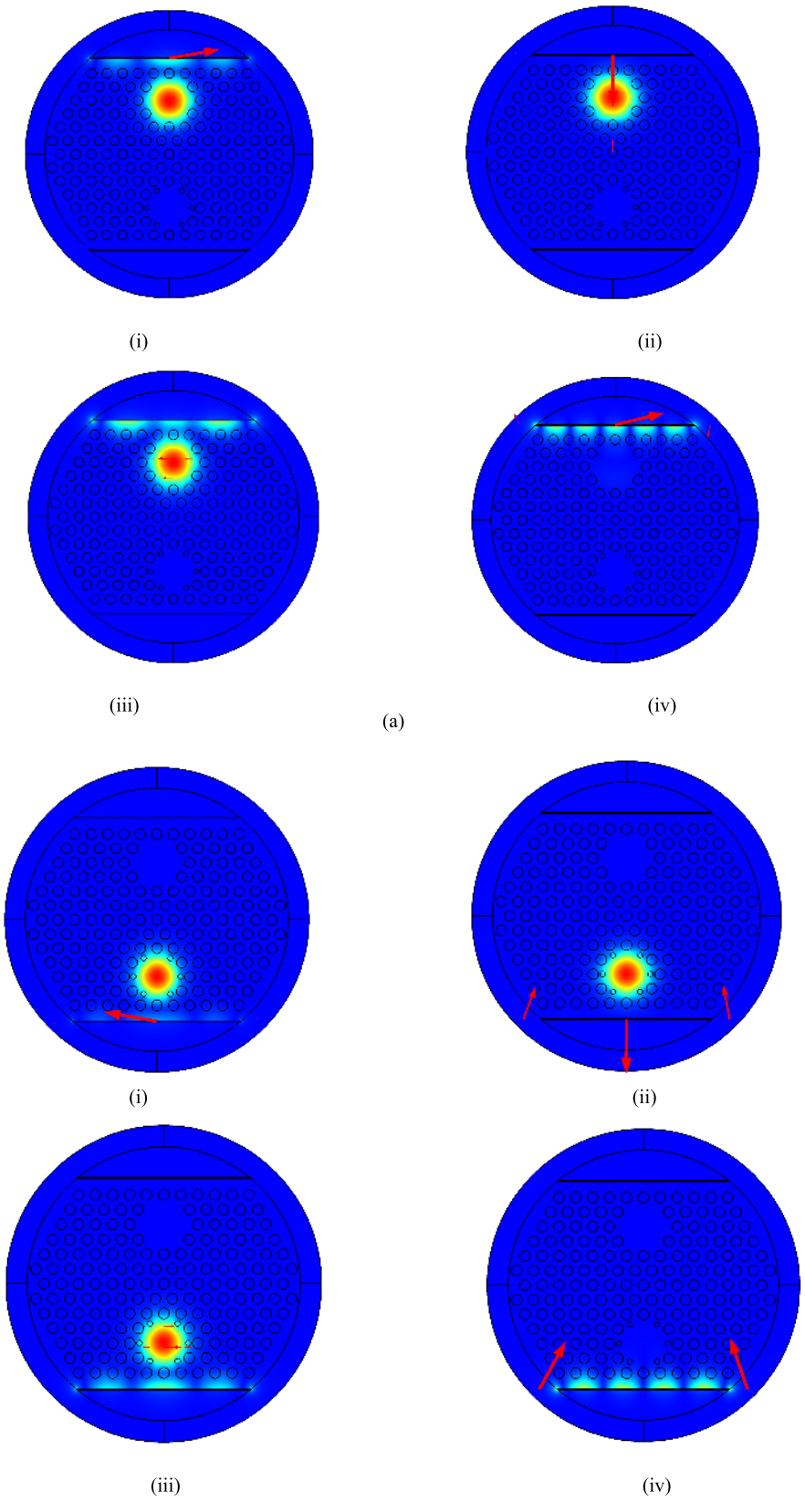

Fig. 3. (a) Electric field distribution of Ch 1: (i) X polarized mode; (ii) Y polarized mode; (iii) coupling mode; (iv) plasmon mode; (b) Electric field distribution of Ch 2:(i) X polarized mode; (ii) Y polarized mode; (iii) coupling mode; (iv) plasmon mode.

is the preferred plasmonic material in most sensor applications due to its chemical stability, biocompatibility, sustained high sensitivity, sharp resonant peak, and excellent accuracy [41]. On the other hand, silver is known to be unstable due to its

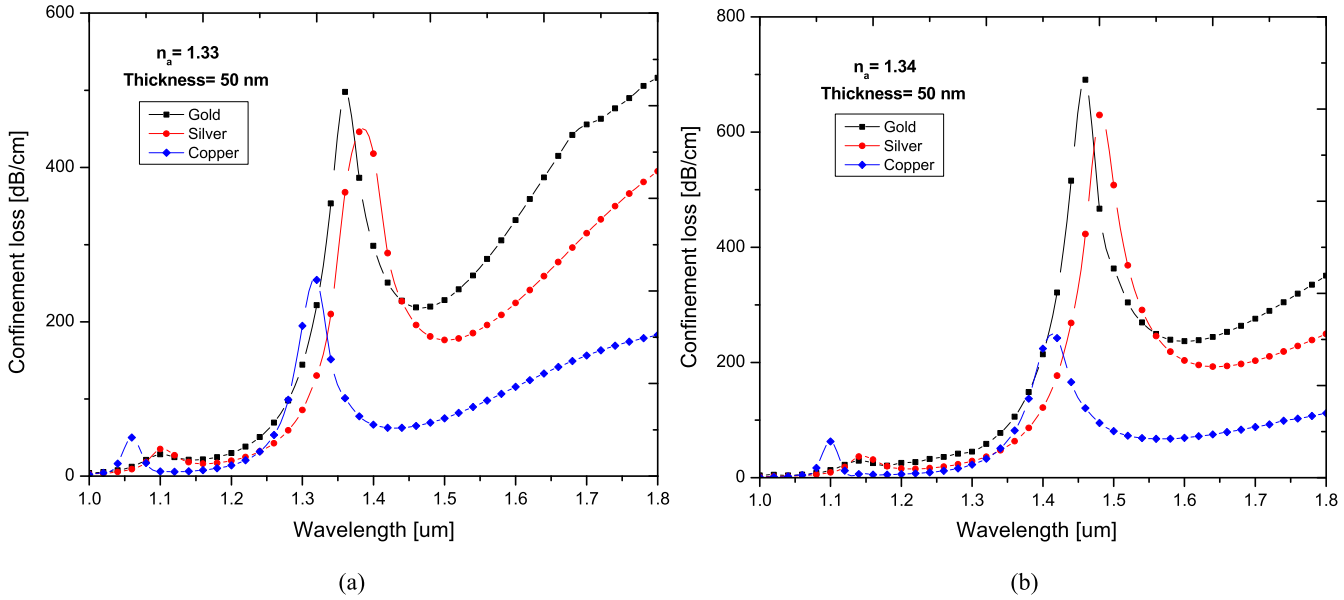

Fig. 4. Confinement loss spectra for different plasmonic materials for (a) Ch1; (b) Ch2.

susceptibility to oxidation, which can negatively impact its accuracy as a plasmonic material. Therefore, additional metal coatings are typically required to mitigate the oxidization issue, resulting in increased manufacturing costs and fabrication complexity [42]. In recent years, there has been extensive research conducted on different plasmonic materials, with a particular focus on their suitability for sensing applications. Among these materials, gold has consistently emerged as the most appropriate choice, as supported by various studies [43], [44], [45], [46]. One notable study conducted by Deepak kumar et al. in 2023 focused on investigating the properties of different plasmonic materials, including gold, silver, copper, aluminium, and a gold-tin alloy. The study specifically calculated the amplitude and wavelength sensitivities for each material, yielding the following results: silver exhibited a sensitivity of 1799nm/RIU, gold had a sensitivity of 1830.76nm/RIU, aluminium had a sensitivity of 1732nm/RIU, copper had a sensitivity of 1652nm/RIU, and the gold-tin alloy had a sensitivity of 1532.2nm/RIU. The study revealed that among the materials examined, gold exhibited the highest sensitivity, making it the preferred plasmonic material for many sensor applications [47].

In the proposed structure, the performance of the sensor in terms of confinement loss is being analyzed using three different metals: gold, silver, and copper. The confinement loss spectra for these plasmonic metals in relation to Ch1 and Ch2 are depicted in Figs. 4 (a,b). The results of the analysis indicate that among the three metals, gold exhibits the maximum confinement loss. This is attributed to the fact that gold provides the highest coupling between the core mode and plasmon mode, resulting in enhanced confinement loss characteristics. As a result, gold is chosen as the plasmonic metal in this proposed sensor based on its superior performance in terms of confinement loss.

C. Optimization of Geometrical Parameters

The objective of the analysis is to examine how various geometrical structural parameters, including air hole diameter (d), pitch size (Λ), gold layer thickness (t_{Au}), and PML layer thickness (t_{PML}) affect the confinement loss. This wavelength-dependent measure is crucial in optimizing sensor performance.

1) Air Hole Diameter Optimization: The sensing performance of the sensor is greatly influenced by the airhole diameter, as these air holes establish the pathway between the core and the metal surface, thereby playing a crucial role in the overall functionality. The investigation involves exploring the ideal air hole diameter by varying it within the range of 0.4μm, 0.5μm, and 0.6μm. Figs.5(a,b) depict the confinement loss spectra for Ch1 and Ch2 across different air hole diameters, plotted against the corresponding wavelengths. When larger air holes are employed, a significant portion of light is effectively guided within the core, leading to reduced interaction between the core mode and plasmon mode and consequently resulting in lower confinement loss. On the other hand, smaller air holes create a larger pathway between the core mode and plasmon mode, leading to a higher degree of confinement loss due to light leakage. However, it is important to note that, in comparison to both 0.5 μm and 0.4 μm air hole diameters, the 0.5 μm diameter air holes can generate a sharp spectrum. This sharp peak is particularly advantageous for efficient sensing in sensors. Hence, to achieve optimal sensitivity, the 0.5 μm air hole diameter is preferred.

2) Pitch Size Optimization: The pitch values are being adjusted to investigate how the pitch size affects the confinement loss characteristics while keeping the other structural parameters constant. Three different values of Λ (0.78 μm, 0.8 μm, and 0.82 μm) are being considered for analyzing the confinement loss. The highest coupling between the core mode and plasmon mode is obtained at the pitch value of 0.8 μm, which gives a sharp peak. Figs. 6 (a, b) depicts the results of Ch1 and Ch2, respectively, illustrating the confinement loss characteristics at different pitch sizes.

3) Gold Layer Thickness Optimization: The gold layer thickness can significantly impact the plasmonic features and

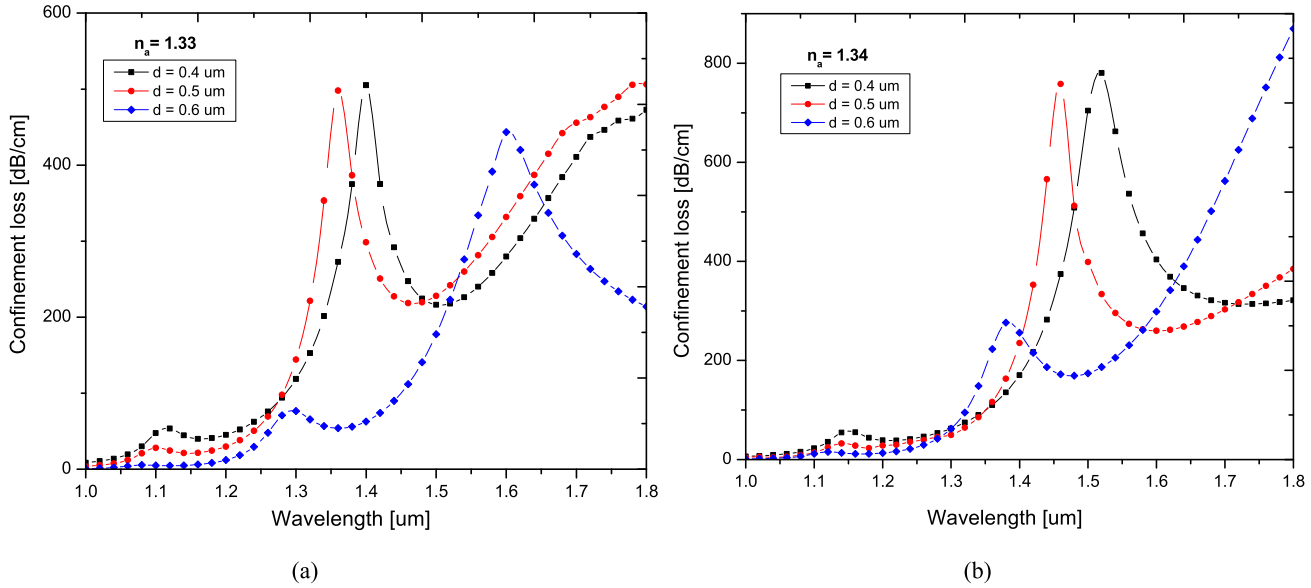

Fig. 5. Confinement loss spectra for air hole diameter variations of (a) Ch1; (b) Ch2.

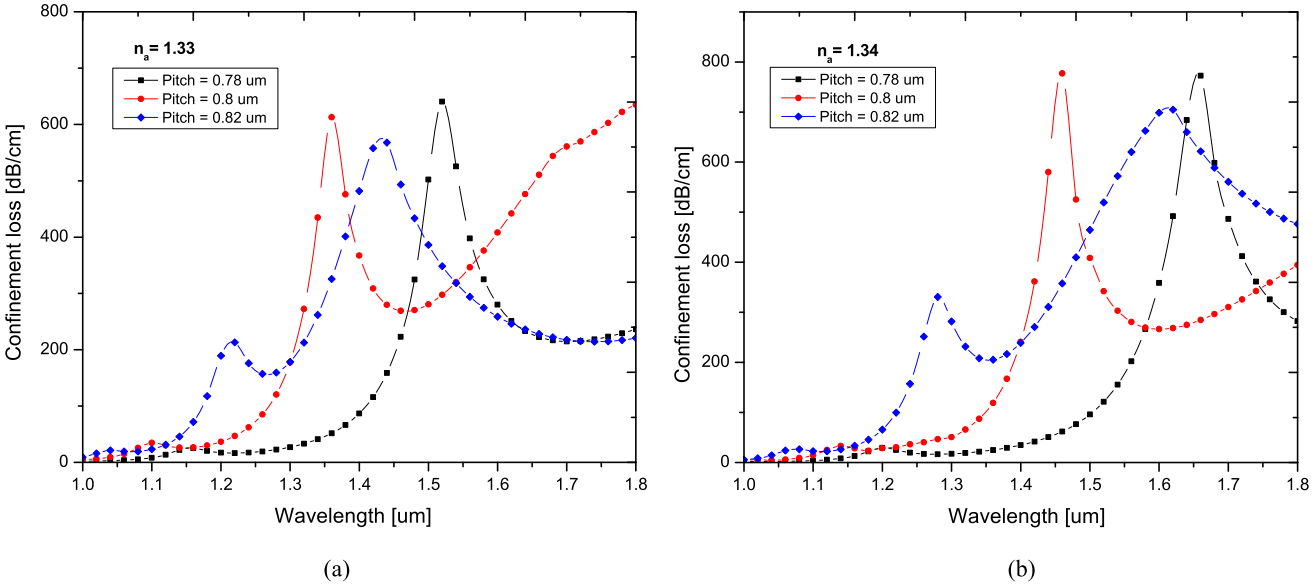

Fig. 6. Confinement loss spectra for pitch size variation of (a) Ch1; (b) Ch2.

efficacy of the sensor [41]. The optimal gold layer thickness is investigated by varying it between 40nm, 50nm, and 60nm. Figs. 7(a,b) display the confinement loss spectra for Ch1 and Ch2 at varying gold layer thicknesses, plotted against the wavelength. The graphs illustrate that increasing the thickness of the gold layer causes the resonance wavelength to shift towards shorter wavelengths. Moreover, there is a reduction in coupling efficiency. Maximum confinement losses of 498.00 dB/cm for Ch1 and 690.73 dB/cm for Ch2 are seen at a gold layer thickness of 50nm, hence, this thickness is used for further analysis.

4) PML Thickness Optimization: The PML layer is used to minimize the reflection of light and reduce scattering losses at the PCF boundary. Increasing the percentage of the PML layer improves phase matching, leading to reduced reflection losses and enhanced PCF performance. A PML layer thickness of 5% to 15% of the PCF diameter enables better mode matching, resulting in decreased reflection losses at the boundary [48]. This study examines various thicknesses of PML that correspond to 5%, 10%, and 15% of the total diameter. The objective is to assess their impact on confinement loss. The findings, depicted in Figs. 8 (a,b) for Ch1 and Ch2, clearly demonstrate that a PML thickness of 10% provides tight confinement, which enhances phase matching and results in higher confinement loss. These results suggest that opting for a PML layer with a thickness of approximately 10% (around 1 μm) can offer advantages in terms of achieving improved mode matching and minimizing reflection losses, particularly in sensing applications.

D. Analysis of Sensor Performance

The detection mechanism of the SPR based PCF sensor relies on the degree of coupling between the plasmon mode and core mode. The confinement loss and resonance

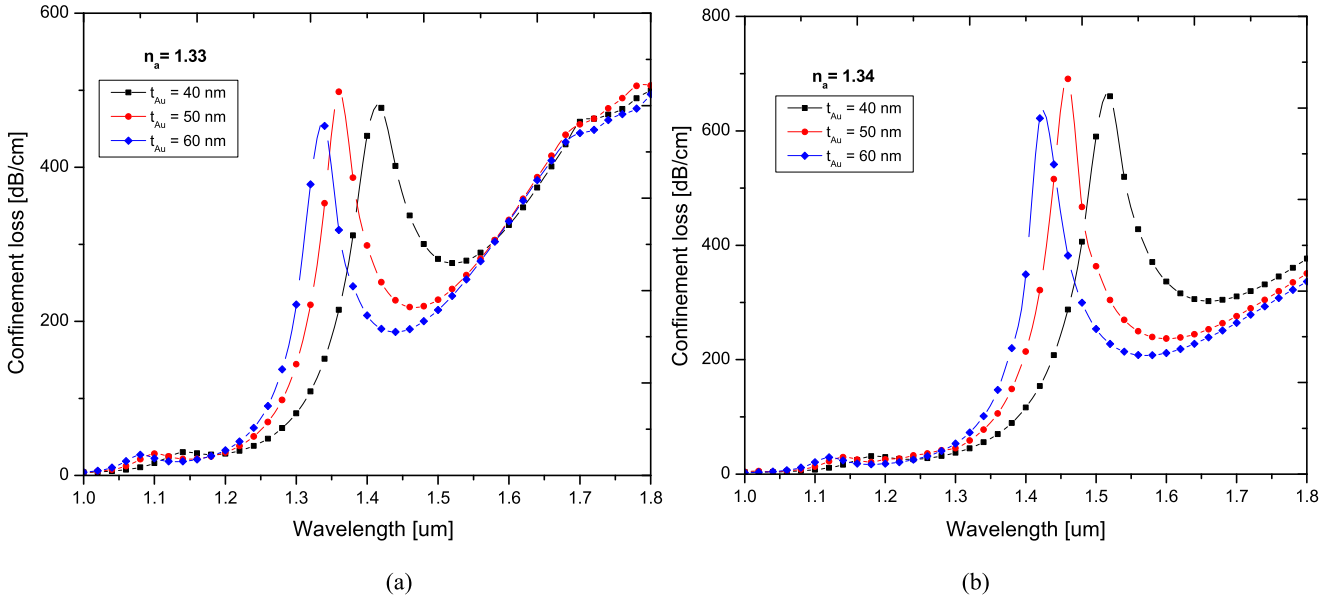

(a) (b)

Fig. 7. Confinement loss spectra for gold layer thickness variations of (a) Ch1; (b) Ch2.

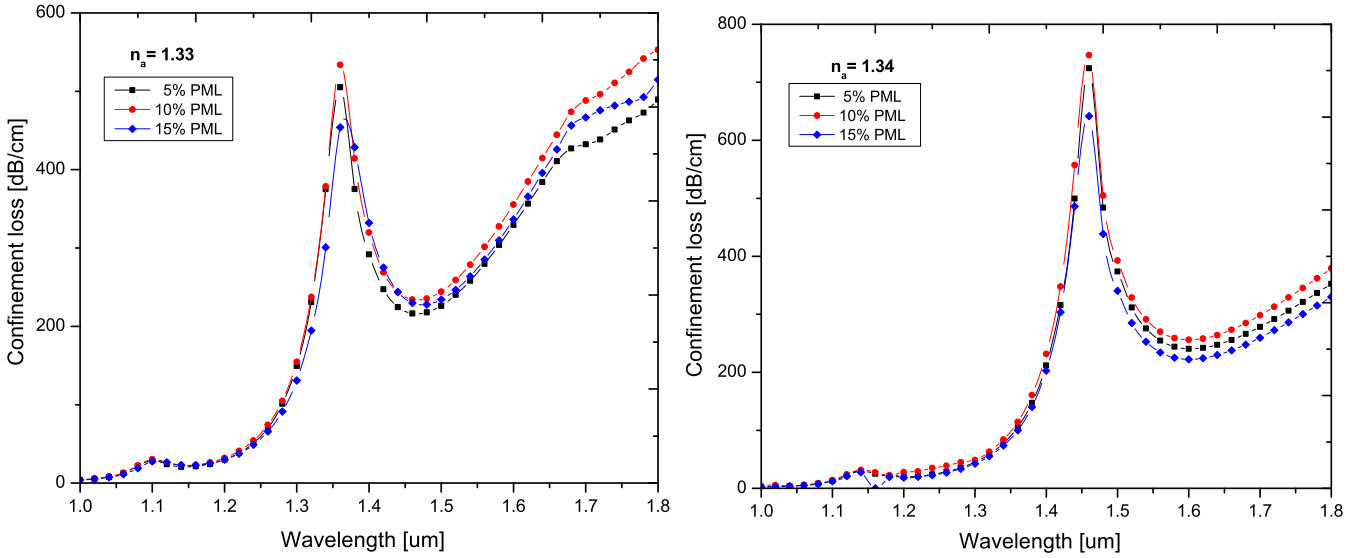

(a) (b)

Fig. 8. Confinement loss spectra for PML layer thickness variations of (a) Ch1; (b) Ch2.

wavelength are fundamental characteristics that play a crucial role in detecting and identifying an unknown analyte [49]. Sensitivity is a significant parameter in SPR sensing, and it measures the resonance wavelength change because of analyte's RI variation. PCF-based SPR sensors offer high sensitivity because they can confine light within the sensing layer, leading to a greater interaction area and improved sensitivity to RI changes. When the RI of the analyte varies, either the resonance peak magnitude or the resonance wavelength moves to a higher or lower wavelength. The efficacy of the sensor depends on its sensitivity, which can be evaluated using two sensing techniques: wavelength sensitivity and amplitude sensitivity. Below is the formula to calculate sensitivity based on wavelength [49],

$$s_\lambda = \frac{\Delta\lambda_{Peak}}{\Delta n_a} (nm/RIU)$$

where, $\Delta\lambda$ peak represents the peak wavelength shift, Δn_a is the change of the analyte RI.

The sensor's amplitude sensitivity is obtained using the equation below [50],

$$s_a = -\frac{\Delta_a(\lambda, n_a)/\Delta n_a}{a(\lambda, n_a)} (RIU^{-1})$$

where $\Delta_a(\lambda, n_a)$ represent the loss spectrum difference between contiguous analyte RI values, $a(\lambda, n_a)$ is the overall maximum loss and Δn_a is the change of the analyte RI.

Figs. 9(a, b) illustrate the confinement loss spectra and amplitude sensitivity of a proposed D-shaped dual channel PCF-based SPR sensor as a function of wavelength between Ch1 and Ch2. The RI values of Ch1(n_a) and Ch2(n_b) are kept at 1.33 and 1.34, respectively for the purpose of this analysis. Ch1 reached its highest resonance point at 1.36 μm, while

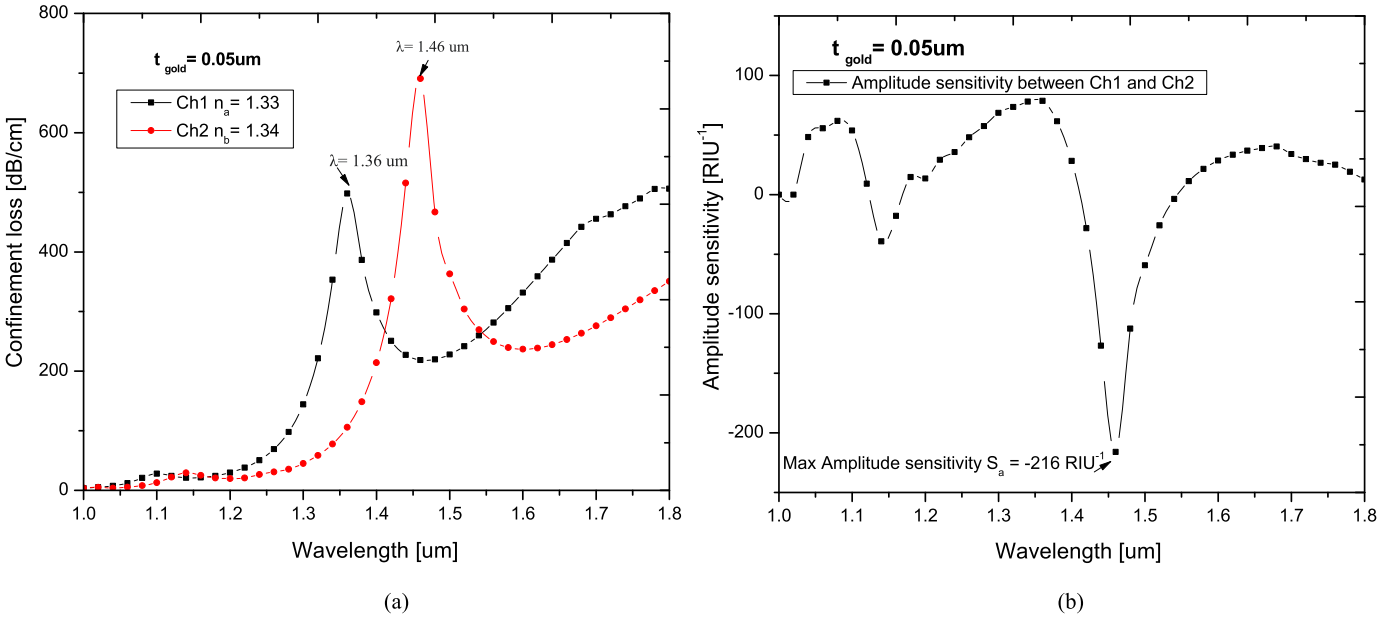

Fig. 9. (a) Confinement loss spectra of Ch1 and Ch2 as a function of wavelength; (b) Amplitude sensitivity between Ch1 and Ch2 as a function of wavelength.

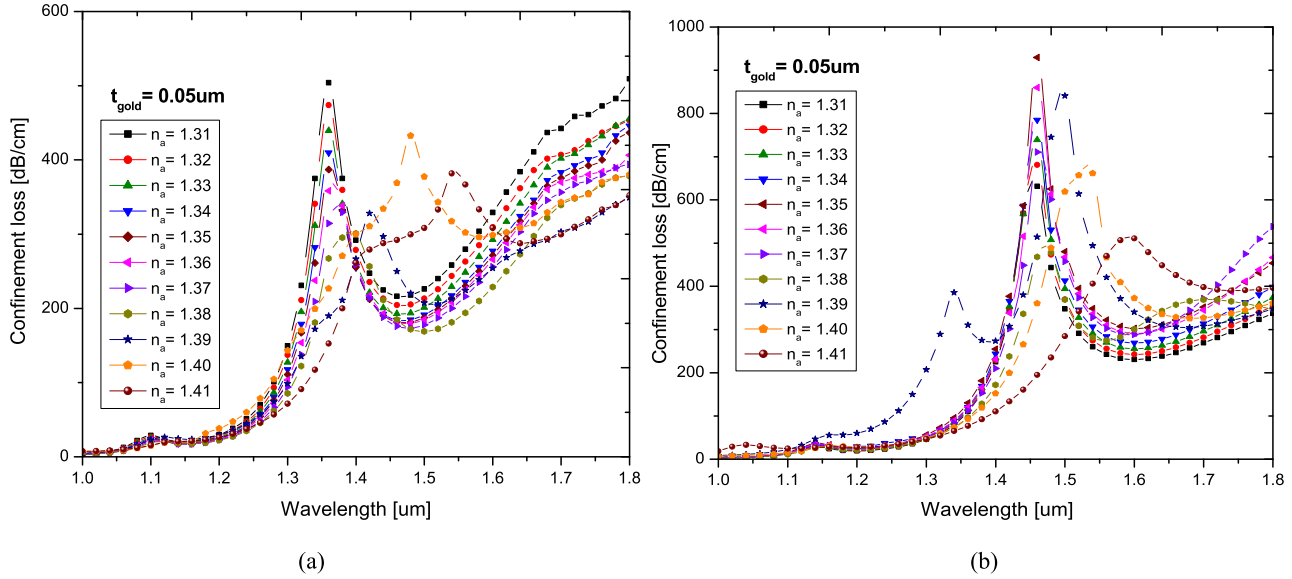

Fig. 10. Confinement loss spectra for different RI values for: (a) Ch1; (b) Ch2.

Ch2 is minimal at this point. On the other hand, Ch2 shows its maximum resonance peak at 1.46 μm, while Ch1 is minimal at this point. This single window detection method achieves high sensitivity and selectivity while minimizing background noise from other regions of the sensor. Ch1 exhibits a peak confinement loss of 498 dB/cm at 1.36 μm, while Ch2 demonstrates a peak confinement loss of 690.73 dB/cm at 1.46 μm. The channels attained a highest wavelength sensitivity of 10000 nm/RIU and an amplitude sensitivity of-216 RIU^{-1} between Ch1 and Ch2.

The proposed sensor's performance is evaluated by testing the RI variations in both channels. Initially, Ch1 is investigated for different analyte variations while keeping the RI value of Ch2 kept at 1.34. Subsequently, Ch2 is investigated with different RI values while keeping the RI value of Ch1 kept at 1.33. Figs. 10(a, b) presents the confinement loss spectra of Ch1 and Ch2 for the proposed sensor, which were numerically investigated for a range of RI values from 1.31 to 1.41 in increments of 0.01. Ch1 showed a decrease in the magnitude of the resonance peak as the RI assorted from 1.31 to 1.36, followed by the shift to longer wavelengths. The maximum confinement loss of 505.23 dB/cm has observed at 1.36 μm for the RI value of 1.31. On the other hand, Ch2 exhibited an opposite trend, with the magnitude of the resonance peak increasing as the RI increased from 1.31 to 1.35 and then decreasing until 1.37. At 1.46 μm wavelength, the optimum confinement loss of 743.59 dB/cm is attained for the RI value of 1.35, whereas for RI values above 1.37, the

TABLE I
PERFORMANCE ANALYSIS OF THE PROPOSED SENSOR FOR DIFFERENT RI VALUES ACCORDING TO CHANNELS

Channel	Refractive index (n)	Resonance wavelength (nm)	Confinement loss (dB/cm)	Wavelength sensitivity (nm/RIU)	Amplitude Sensitivity [RIU^{-1}]	Resolution (RIU)	FOM [RIU^{-1}]
Ch1	1.31	1360	505.23	NA	-3.04	-	NA
	1.32	1360	502.54	-	-2.79	-	-
	1.33	1360	498.00	-	-4.14	-	-
	1.34	1360	491.51	-	-4.92	-	-
	1.35	1360	477.52	-	-6.57	-	-
	1.36	1360	453.95	-	-7.62	$5x10^{-5}$	-
	1.37	1380	439.39	2000	-26.03	$5x10^{-5}$	37.73
	1.38	1400	421.38	2000	-39.08	$5x10^{-5}$	28.57
	1.39	1420	393.69	2000	-85.39	$1.67x10^{-5}$	43.47
	1.40	1480	490.19	6000	-48.58	$1.67x10^{-5}$	125
	1.41	1540	445.41	6000	NA	NA	93.75
Ch2	1.31	1460	631.40	NA	-3.92	-	NA
	1.32	1460	653.51	-	-4.31	-	-
	1.33	1460	679.86	-	-36.26	-	-
	1.34	1460	690.73	-	-25.39	-	-
	1.35	1460	743.59	-	-9.25	-	-
	1.36	1460	730.72	-	-23.05	-	-
	1.37	1460	639.53	-	-37.30	$5x10^{-5}$	-
	1.38	1480	525.70	2000	-304.52	$5x10^{-5}$	50
	1.39	1500	714.97	2000	-80.86	$2.5x10^{-5}$	66.67
	1.40	1540	562.15	4000	-261.15	$2.55x10^{-5}$	68.96
	1.41	1600	408.75	6000	NA	NA	57.14

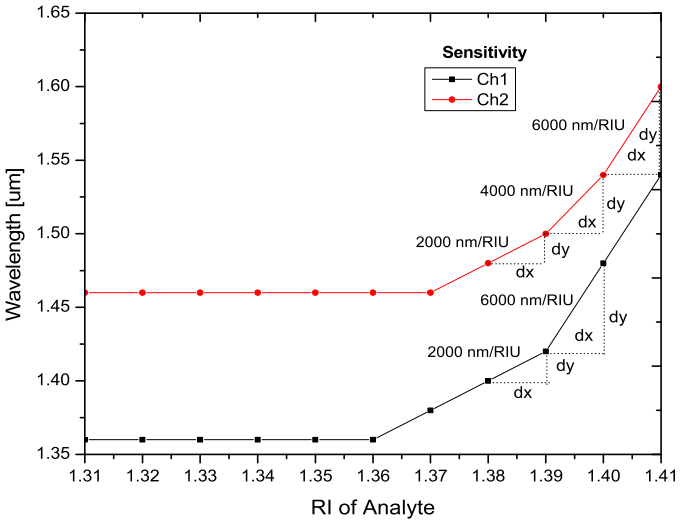

Fig. 11. Wavelength sensitivity analysis of different analyte RI value for Ch1 and Ch2.

resonance peak shifts towards longer wavelengths. Notably, the proposed sensor structure possesses the ability to measure both amplitude and wavelength sensitivity, thereby providing enhanced performance characteristics. Additionally, Ch1 and Ch2 individually achieved an optimal wavelength sensitivity of 6000 nm/RIU. Fig. 11 depicted wavelength sensitivity analysis of the proposed sensor for Ch1 and Ch2.

Figs. 12(a, b) illustrate the amplitude sensitivity with respect to changes in wavelength for different analyte RI values in Ch1 and Ch2. As the RI of analyte increases in Ch1, the resonance peak moves towards higher wavelengths, and observed an optimal amplitude sensitivity of -87.39 RIU^{-1}. Alternatively, Ch2 exhibits a shift in the resonance peak towards shorter wavelengths with increasing analyte RI, coupled with an optimal amplitude sensitivity of -304.52 RIU^{-1}. Table I illustrates the proposed sensor's performance analysis for both Ch1 and Ch2 with varying analyte RI values.

The sensor's resolution determines its ability to identify minor alterations in the analyte's RI. The following equation shows the measure of minimum observable RI limit [19],

$$\text{Resolution} = \Delta n_{aX} \frac{\Delta\lambda_{min}}{\Delta\lambda_{Peak}} (\text{RIU})$$

The spectral resolution is set at a minimum of 0.1 nm, indicated by $\Delta\lambda_{min}$. Meanwhile, $\Delta\lambda_{peak}$ and Δn_a represent the peak wavelength shift and analyte's RI change, respectively. The maximum resolution measured using the proposed sensor is 5×10^{-5} RIU for both Ch1 and Ch2, it is evident that the proposed sensor can identify minor RI changes.

The figure of merit (FOM) for the sensor is a vital parameter that is determined by dividing the sensitivity with full width at half maximum (FWHM). The optimal FOM measured using the proposed sensor for Ch1, Ch2 is 125 RIU and 68.96 RIU, respectively. This value can be calculated using the following equation [19]:

$$\text{FOM} = \frac{s_\lambda (nm/RIU)}{FWHM(nm)} (\text{RIU}^{-1})$$

The performance of the proposed sensor demonstrated significant improvements compared to the existing literature. Table II

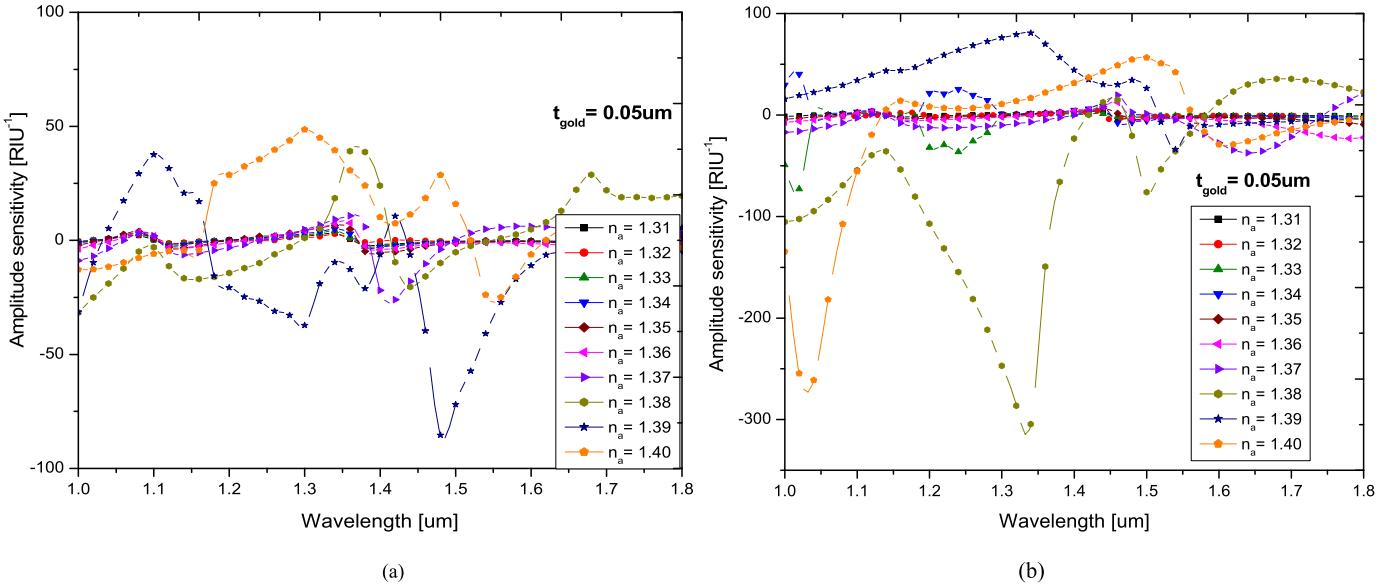

Fig. 12. Amplitude sensitivity spectra for different RI values for: (a) Ch1; (b) Ch2.

TABLE II
COMPARATIVE ANALYSIS OF THE PRESENTED SENSOR WITH RECENTLY PUBLISHED PCF BASED SPR SENSORS

Ref	Structure	RI range	Wavelength sensitivity (nm/RIU)	Resolution (RIU)
[25]	Two channels	1.30-1.40	Ch1- 1000 Ch2- 3750	NA
[26]	Two channels	1.33-1.366	Ch1- 2500 Ch2- 3083	Ch1- 4×10^{-5} Ch2-3.2×10^{-5}
[27]	Two channels	1.34-1.37	Ch1- 4100 Ch2- 3820	Ch1- 3.3×10^{-5} Ch2- 6.3×10^{-5}
[51]	Two channels	1.33-1.36	Ch1- 3500 Ch2- 3500	NA
[52]	Two channels	1.34-1.36	Ch1- 4280 Ch2 -3940	Ch1- 2.34×10^{-5} Ch2- 2.54×10^{-5}
[18]	Four channels	1.33-1.34	Ch1- 2200 Ch2- 2400 Ch3- 2200 Ch4- 2400	NA
[53]	Four channels	1.33-1.43	Ch1- 1340 Ch2- 1465 Ch3- 1590 Ch4- 1795	NA
Proposed work	Two channels	1.31-1.41	Ch1- 6000 Ch2- 6000 Maximum- 10000	Ch1- 5×10^{-5} Ch2- 5×10^{-5}

presents a performance comparison between the presented sensor and the most recent publications. It is clear that our suggested sensor surpasses the existing sensors Additionally, the proposed sensor has a broad detection range, enabling it to detect various analyte RIs.

IV. CONCLUSION

This article proposed a novel dual-channel plasmonic sensor that utilizes a D-shaped PCF for detecting two different analytes simultaneously. The sensor design incorporates a dual-core structure to enable the analysis of two different analytes simultaneously. The core section is formed by eliminating one ring of air holes at the bottom and two rings at the top, while the birefringence is attained by halving the size of the second air hole rings in the bottom core region. Additionally, the top and bottom circular portions of the fiber are removed to form a dual D-shaped structure. The SPR effect is initiated by depositing a 50 nm thick gold layer on both planar sides of the PCF, and the analyte is placed above it in Ch1 and Ch2. Numerical analyses are performed using FEM. After optimizing the sensor structure, it attains optimal wavelength sensitivity of 10000 nm/RIU and amplitude sensitivity of -216 RIU^{-1} between Ch1 and Ch2. Both channels exhibit distinct sensitivity ranges, where Ch1 shows a maximal amplitude sensitivity of -85.39 RIU^{-1} over the RI value of 1.31 to 1.40 and maximal wavelength sensitivity of 6000 nm/RIU with a resolution of 5×10^{-5} in the range of 1.37 to 1.41, while Ch2 demonstrates a maximal amplitude sensitivity of -304.52 RIU^{-1} over the RI value of 1.31 to 1.40 and maximal wavelength sensitivity of 6000 nm/RIU with

a resolution of 5×10^{-5} in the range of 1.38 to 1.41. This novel sensor offers a wide detection range, making it appropriate for diverse sensing applications such as chemical, biological, and industrial sensing.

REFERENCES

[1] J. Homola, S. S. Yee, and G. Gauglitz, "Surface plasmon resonance sensors: Review," *Sens. Actuators, B, Chem.*, vol. 54, nos. 1–2, pp. 3–15, 1999, doi: 10.1016/S0925-4005(98)00321-9.

[2] A. K. Sharma, A. K. Pandey, and B. Kaur, "A review of advancements (2007–2017) in plasmonics-based optical fiber sensors," *Opt. Fiber Technol.*, vol. 43, pp. 20–34, Jul. 2018, doi: 10.1016/j.yofte.2018.03.008.

[3] E. Kretschmann and H. Raether, "Radiative decay of non radiative surface plasmons excited by light," *Zeitschrift Für Naturforschung A*, vol. 23, no. 12, pp. 2135–2136, Dec. 1968, doi: 10.1515/zna-1968-1247.

[4] V. Yesudasu, H. S. Pradhan, and R. J. Pandya, "Recent progress in surface plasmon resonance based sensors: A comprehensive review," *Heliyon*, vol. 7, no. 3, Mar. 2021, Art. no. e06321, doi: 10.1016/j.heliyon.2021.e06321.

[5] R. Otupiri, E. K. Akowuah, and S. Haxha, "Multi-channel SPR biosensor based on PCF for multi-analyte sensing applications," *Opt. Exp.*, vol. 23, no. 12, 2015, Art. no. 15716, doi: 10.1364/oe.23.015716.

[6] Y. Singh, M. K. Paswan, and S. K. Raghuwanshi, "Sensitivity enhancement of SPR sensor with the black phosphorus and graphene with bi-layer of gold for chemical sensing," *Plasmonics*, vol. 16, no. 5, pp. 1781–1790, Oct. 2021, doi: 10.1007/s11468-020-01315-3.

[7] P. Falkowski, Z. Lukaszewski, and E. Gorodkiewicz, "Potential of surface plasmon resonance biosensors in cancer detection," *J. Pharmaceutical Biomed. Anal.*, vol. 194, Feb. 2021, Art. no. 113802, doi: 10.1016/j.jpba.2020.113802.

[8] M. Mahmoudpour, J. E. N. Dolatabadi, M. Torbati, and A. Homayouni-Rad, "Nanomaterials based surface plasmon resonance signal enhancement for detection of environmental pollutions," *Biosensors Bioelectron.*, vol. 127, pp. 72–84, Feb. 2019, doi: 10.1016/j.bios.2018.12.023.

[9] L. Zhang et al., "Development of a surface plasmon resonance and fluorescence imaging system for biochemical sensing," *Micromachines*, vol. 10, no. 7, p. 442, Jul. 2019.

[10] M. R. Islam et al., "Trigonal cluster-based ultra-sensitive surface plasmon resonance sensor for multipurpose sensing," *Sens. Bio-Sens. Res.*, vol. 35, Feb. 2022, Art. no. 100477, doi: 10.1016/j.sbsr.2022.100477.

[11] M. R. Islam, A. N. M. Iftekher, K. R. Hasan, M. J. Nayen, and S. B. Islam, "Dual-polarized highly sensitive surface-plasmon-resonance-based chemical and biomolecular sensor," *Appl. Opt.*, vol. 59, no. 11, p. 3296, 2020, doi: 10.1364/ao.383352.

[12] A. Hassani and M. Skorobogatiy, "Design of the microstructured optical fiber-based surface plasmon resonance sensors with enhanced microfluidics," *Opt. Exp.*, vol. 14, no. 24, 2006, Art. no. 11616, doi: 10.1364/oe.14.011616.

[13] T. Yang, L. Zhang, Y. Shi, S. Liu, and Y. Dong, "A highly birefringent photonic crystal fiber for terahertz spectroscopic chemical sensing," *Sensors*, vol. 21, no. 5, pp. 1–12, 2021, doi: 10.3390/s21051799.

[14] B. K. Paul, K. Ahmed, D. Vigneswaran, F. Ahmed, S. Roy, and D. Abbott, "Quasi-photonic crystal fiber-based spectroscopic chemical sensor in the terahertz spectrum: Design and analysis," *IEEE Sensors J.*, vol. 18, no. 24, pp. 9948–9954, Dec. 2018, doi: 10.1109/JSEN.2018.2872892.

[15] B. K. Paul et al., "Investigation of gas sensor based on differential optical absorption spectroscopy using photonic crystal fiber," *Alexandria Eng. J.*, vol. 59, no. 6, pp. 5045–5052, Dec. 2020, doi: 10.1016/j.aej.2020.09.030.

[16] K. V. Kumar, K. C. Ramya, S. Karthikumar, and K. K. Kumar, "Design of temperature sensor using twisted photonic crystal fiber," *Results Phys.*, vol. 10, pp. 856–857, Sep. 2018, doi: 10.1016/j.rinp.2018.08.005.

[17] V. Kaur and S. Singh, "D-shaped photonic crystal fiber based surface plasmon resonance sensor using dual coating of metal oxide for healthcare applications," in *Proc. IEEE 16th Nanotechnol. Mater. Devices Conf. (NMDC)*, Dec. 2021, pp. 1–4, doi: 10.1109/NMDC50713.2021.9677553.

[18] S. I. Azzam, M. F. O. Hameed, R. E. A. Shehata, A. M. Heikal, and S. S. A. Obayya, "Multichannel photonic crystal fiber surface plasmon resonance based sensor," *Opt. Quantum Electron.*, vol. 48, no. 2, pp. 1–11, Feb. 2016, doi: 10.1007/s11082-016-0414-4.

[19] N. Ayyanar, K. V. Sreekanth, G. T. Raja, and M. S. M. Rajan, "Photonic crystal fiber-based reconfigurable biosensor using phase change material," *IEEE Trans. Nanobiosci.*, vol. 20, no. 3, pp. 338–344, Jul. 2021, doi: 10.1109/TNB.2021.3065006.

[20] S. Selvendran, A. S. Raja, and S. Yogalakshmi, "A highly sensitive surface plasmon resonance biosensor using photonic crystal fiber filled with gold nanowire encircled by silicon lining," *Optik*, vol. 156, pp. 112–120, Mar. 2018, doi: 10.1016/j.ijleo.2017.10.157.

[21] A. A. Rifat, R. Ahmed, G. A. Mahdiraji, and F. R. M. Adikan, "Highly sensitive D-shaped photonic crystal fiber-based plasmonic biosensor in visible to near-IR," *IEEE Sensors J.*, vol. 17, no. 9, pp. 2776–2783, May 2017.

[22] H. Yang et al., "Highly sensitive graphene-Au coated plasmon resonance PCF sensor," *Sensors*, vol. 21, no. 3, pp. 1–14, 2021, doi: 10.3390/s21030818.

[23] M. E. Rahaman, R. H. Jibon, M. S. Ahsan, F. Ahmed, and I.-B. Sohn, "Glucose level measurement using photonic crystal fiber–based plasmonic sensor," *Plasmonics*, vol. 17, no. 1, pp. 1–11, Feb. 2022, doi: 10.1007/s11468-021-01497-4.

[24] Y. Zhang, C. Zhou, L. Xia, X. Yu, and D. Liu, "Wagon wheel fiber based multichannel plasmonic sensor," *Opt. Exp.*, vol. 19, no. 23, 2011, Art. no. 22863, doi: 10.1364/oe.19.022863.

[25] V. Kaur and S. Singh, "A dual-channel surface plasmon resonance biosensor based on a photonic crystal fiber for multianalyte sensing," *J. Comput. Electron.*, vol. 18, no. 1, pp. 319–328, Mar. 2019, doi: 10.1007/s10825-019-01305-7.

[26] A. Yasli, H. Ademgil, S. Haxha, and A. Aggoun, "Multi-channel photonic crystal fiber based surface plasmon resonance sensor for multi-analyte sensing," *IEEE Photon. J.*, vol. 12, no. 1, pp. 1–15, Feb. 2020, doi: 10.1109/JPHOT.2019.2961110.

[27] A. Yasli and H. Ademgil, "Multianalyte sensing analysis with multilayer photonic crystal fiber-based surface plasmon resonance sensor," *Modern Phys. Lett. B*, vol. 34, no. 33, Nov. 2020, Art. no. 2050375, doi: 10.1142/S0217984920503753.

[28] Q. M. Kamrunnahar et al., "Plasmonic micro-channel assisted photonic crystal fiber based highly sensitive sensor for multi-analyte detection," *Nanomaterials*, vol. 12, no. 9, p. 1444, Apr. 2022, doi: 10.3390/nano12091444.

[29] J. Sultana et al., "Exploring low loss and single mode in antiresonant tube lattice terahertz fibers," *IEEE Access*, vol. 8, pp. 113309–113317, 2020, doi: 10.1109/ACCESS.2020.3003035.

[30] M. T. Islam, M. G. Moctader, K. Ahmed, and S. Chowdhury, "Benzene shape photonic crystal fiber based plasma sensor: Design and analysis," *Photonic Sensors*, vol. 8, no. 3, pp. 263–269, Sep. 2018, doi: 10.1007/s13320-018-0495-8.

[31] D. Pysz et al., "Stack and draw fabrication of soft glass microstructured fiber optics," *Bull. Polish Acad. Sci. Tech. Sci.*, vol. 62, no. 4, pp. 667–682, Dec. 2014, doi: 10.2478/bpasts-2014-0073.

[32] T. Huang, "Highly sensitive SPR sensor based on D-shaped photonic crystal fiber coated with indium tin oxide at near-infrared wavelength," *Plasmonics*, vol. 12, no. 3, pp. 583–588, Jun. 2017, doi: 10.1007/s11468-016-0301-7.

[33] J. Boehm, A. François, H. Ebendorff-Heidepriem, and T. M. Monro, "Chemical deposition of silver for the fabrication of surface plasmon microstructured optical fibre sensors," *Plasmonics*, vol. 6, no. 1, pp. 133–136, Mar. 2011, doi: 10.1007/s11468-010-9178-z.

[34] P. S. Maji and P. Roy Chaudhuri, "A new design for all-normal near zero dispersion photonic crystal fiber with selective liquid infiltration for broadband supercontinuum generation at 1.55 μm," *J. Photon.*, vol. 2014, pp. 1–9, Apr. 2014, doi: 10.1155/2014/728592.

[35] M. R. Islam et al., "Highly birefringent gold-coated SPR sensor with extremely enhanced amplitude and wavelength sensitivity," *Eur. Phys. J. Plus*, vol. 136, no. 2, pp. 1–14, Feb. 2021, doi: 10.1140/epjp/s13360-021-01220-6.

[36] C. Li et al., "Two modes excited SPR sensor employing gold-coated photonic crystal fiber based on three-layers air-holes," *IEEE Sensors J.*, vol. 20, no. 11, pp. 5893–5899, Jun. 2020, doi: 10.1109/JSEN.2020.2972031.

[37] D. Kumar, M. Sharma, and V. Singh, "Surface plasmon resonance implemented silver thin film PCF sensor with multiple—Hole microstructure for wide ranged refractive index detection," *Mater. Today, Proc.*, vol. 62, pp. 6590–6595, Jan. 2022, doi: 10.1016/j.matpr.2022.04.598.

[38] M. F. Azman, G. A. Mahdiraji, W. R. Wong, R. A. Aoni, and F. R. M. Adikan, "Design and fabrication of copper-filled photonic crystal fiber based polarization filters," *Appl. Opt.*, vol. 58, no. 8, p. 2068, 2019, doi: 10.1364/ao.58.002068.

[39] M. R. Islam, A. N. M. Iftekher, M. S. Anzum, M. Rahman, and S. Siraz, "LSPR based double peak double plasmonic layered bent core PCF-SPR sensor for ultra-broadband dual peak sensing," *IEEE Sensors J.*, vol. 22, no. 6, pp. 5628–5635, Mar. 2022, doi: 10.1109/JSEN.2022.3149715.

[40] V. Sorathiya, S. Lavadiya, O. S. Faragallah, M. M. A. Eid, and A. N. Z. Rashed, "D shaped dual core photonics crystal based refractive index sensor using graphene–titanium–silver materials for infrared frequency spectrum," *Opt. Quantum Electron.*, vol. 54, no. 5, pp. 1–13, May 2022, doi: 10.1007/s11082-022-03700-0.

[41] M. R. Islam et al., "Design and numerical analysis of a gold-coated photonic crystal fiber based refractive index sensor," *Opt. Quantum Electron.*, vol. 53, no. 2, pp. 1–18, Feb. 2021, doi: 10.1007/s11082-021-02748-8.

[42] M. Hasan, S. Akter, A. Rifat, S. Rana, and S. Ali, "A highly sensitive gold-coated photonic crystal fiber biosensor based on surface plasmon resonance," *Photonics*, vol. 4, no. 4, p. 18, Mar. 2017, doi: 10.3390/photonics4010018.

[43] S. Chakma, M. A. Khalek, B. K. Paul, K. Ahmed, M. R. Hasan, and A. N. Bahar, "Gold-coated photonic crystal fiber biosensor based on surface plasmon resonance: Design and analysis," *Sens. Bio-Sens. Res.*, vol. 18, pp. 7–12, Apr. 2018, doi: 10.1016/j.sbsr.2018.02.003.

[44] M. N. Hossen, M. Ferdous, M. A. Khalek, S. Chakma, B. K. Paul, and K. Ahmed, "Design and analysis of biosensor based on surface plasmon resonance," *Sens. Bio-Sens. Res.*, vol. 21, pp. 1–6, Nov. 2018, doi: 10.1016/j.sbsr.2018.08.003.

[45] Q. M. Kamrunnahar, J. R. Mou, and M. Momtaj, "Dual-core gold coated photonic crystal fiber plasmonic sensor: Design and analysis," *Results Phys.*, vol. 18, Sep. 2020, Art. no. 103319, doi: 10.1016/j.rinp.2020.103319.

[46] A. Shafkat, "Analysis of a gold coated plasmonic sensor based on a duplex core photonic crystal fiber," *Sens. Bio-Sens. Res.*, vol. 28, Jun. 2020, Art. no. 100324, doi: 10.1016/j.sbsr.2020.100324.

[47] D. Kumar, M. Khurana, M. Sharma, and V. Singh, "Analogy of gold, silver, copper and aluminium based ultra-sensitive surface plasmon resonance photonic crystal fiber biosensors," *Mater. Today, Proc.*, Mar. 2023, doi: 10.1016/j.matpr.2023.02.319.

[48] B. K. Paul, K. Ahmed, S. Asaduzzaman, and M. S. Islam, "Folded cladding porous shaped photonic crystal fiber with high sensitivity in optical sensing applications: Design and analysis," *Sens. Bio-Sens. Res.*, vol. 12, pp. 36–42, Feb. 2017, doi: 10.1016/j.sbsr.2016.11.005.

[49] N. Jahan et al., "Photonic crystal fiber based biosensor for pseudomonas bacteria detection: A simulation study," *IEEE Access*, vol. 9, pp. 42206–42215, 2021.

[50] N. Luan, L. Zhao, Y. Lian, and S. Lou, "A high refractive index plasmonic sensor based on D-shaped photonic crystal fiber with laterally accessible hollow-core," *IEEE Photon. J.*, vol. 10, no. 5, pp. 1–7, Oct. 2018, doi: 10.1109/JPHOT.2018.2873826.

[51] A. Yasli and H. Ademgil, "Bending analysis of multi-analyte photonic crystal fiber based surface plasmon resonance sensor," *Opt. Quantum Electron.*, vol. 54, no. 3, pp. 1–15, Mar. 2022, doi: 10.1007/s11082-022-03607-w.

[52] S. Jiao, X. Ren, H. Yang, S. Xu, and X. Li, "Dual-channel and dual-core plasmonic sensor–based photonic crystal fiber for refractive index sensing," *Plasmonics*, vol. 17, no. 1, pp. 295–304, Feb. 2022, doi: 10.1007/s11468-021-01518-2.

[53] L. Liu, Z. Liu, Y. Zhang, and S. Liu, "Multi-channel optical fiber surface plasmon resonance sensor with narrow FWHM, high figure of merit, and wide detection range," *Plasmonics*, vol. 17, no. 5, pp. 2235–2244, Oct. 2022, doi: 10.1007/s11468-022-01713-9.